Eur. Phys. J. Plus (2024) 139:893
https://doi.org/10.1140/epjp/s13360-024-05670-6

THE EUROPEAN PHYSICAL JOURNAL PLUS

Regular Article

Measurement of tritium production in the helium cooled pebble bed test blanket module mock-up at JET during DTE2

N. Fonnesu[1,a], M. Angelone[1], S. Loreti[1], M. Pillon[1], R. Villari[1], P. Batistoni[1], A. Colangeli[1], D. Flammini[1], M. Lungaroni[1], F. Moro[1], S. Noce[1], A. Previti[1], X. Litaudon[2], JET Contributors

[1] Nuclear Department, ENEA, Via E. Fermi 45, 00044 Frascati, Rome, Italy
[2] CEA, IRFM, 13108 St-Paul-Lez-Durance, France
[3] EUROfusion Consortium, JET, Culham Science Centre, Abingdon OX14 3DB, UK

Received: 30 July 2024 / Accepted: 19 September 2024

Abstract Quite often, detectors for measuring nuclear performance and radiation quantities of relevance in fusion experiments are requested to withstand harsh working conditions due to intense neutron and gamma radiation fields. High temperature constitutes a further harsh element in some locations of the machine, where it is necessary to perform some on-line measurements, as expected in the breeding blanket. This is an essential component in future fusion power plants to provide tritium self-sufficiency and its performance must be continuously monitored. Some Test Blanket Modules (TBMs) will be installed in ITER to provide the first experimental data to validate the predictions on tritium production and recovery. In the meantime, within EUROfusion program, the mock-up of the Helium Cooled Pebble Bed Test Blanket Module (HCPB TBM), previously used for the TBM experiment at the Frascati Neutron Generator (FNG), had been installed at JET to test some detectors and for benchmarking numerical codes used for breeding blanket assessment during DTE2 campaign. A diamond detector, calibrated to measure the tritium production through neutron detection inside the HCPB TBM mock-up, was tested during some plasma pulses of the DTE2 campaign at JET. The main outcome is that, as far as neutron emission rate is below 10^{15} s^{-1}, neutrons are properly detected along the plasma discharge evolution by TBM diamond detector, consistently with the JET neutron monitor KN1. Moreover, the amount of tritium measured (E) is 1.40×10^{-12} tritons per source neutron and the comparison with MCNP radiation transport simulation (C) gives a ratio $C/E = 0.77$. Such measurements, considered promising, and their comparison with calculations are discussed in the present work. Criticalities emerged are analyzed and some improvements proposed with the main purpose of speeding up signal processing to make the system capable of working at higher plasma neutron emission rates.

1 Introduction

The first deuterium–tritium (DT) campaign at JET, a.k.a. DTE1 [1, 2], occurred in 1997 and since then, significant improvements were made to the machine, among which, the installation of a beryllium first wall and tungsten divertor of relevance for ITER in lieu of the original carbon wall, more additional heating power and an extension of the diagnostics [3]. Such changes have been applied to the tokamak in preparation of the subsequent DTE2 campaign, occurred in the second part of 2021, to exploit the unprecedented ITER-relevant capabilities of JET [4].

The nuclear technology program at JET started with EUROfusion work package (WP) JET3 [5] and continued under WP PrIO (Preparation of ITER operation) [6] has aimed at maximizing the scientific return from the high neutron yield of DTE2. Among the tasks, TBMD (Test Blanket Module Detectors) was established for testing some detectors for tritium breeding blankets. This is because the development of tritium breeding blankets is one of the main challenges on the path of a fusion reactor and Test Blanket Modules (TBMs) in ITER will provide the first experimental data to validate the predictions on tritium production and reliable measurement systems are needed. Considering the operating conditions expected in the TBMs, some detectors capable of working is such a harsh environment are under evaluation. The mock-up of the Helium Cooled Pebble Bed Test Blanket Module (HCPB TBM), previously used for the TBM experiment at the Frascati Neutron Generator (FNG) [7, 8], had been installed at JET and a diamond detector, calibrated to measure tritium production through neutron detection, was located into one of its diagnostic channels. The detector is equipped with a LiF converting layer, to detect thermal neutrons through the creation of charged particles which release their energy in the crystal bulk.

See the author list of "Overview of T and D-T results in JET with ITER-like wall" by CF Maggi et al. to be published in Nuclear Fusion Special Issue: Overview and Summary Papers from the 29th Fusion Energy Conference (London, UK, 16-21 October 2023).

[a] e-mail: nicola.fonnesu@enea.it (corresponding author)

Published online: 14 October 2024

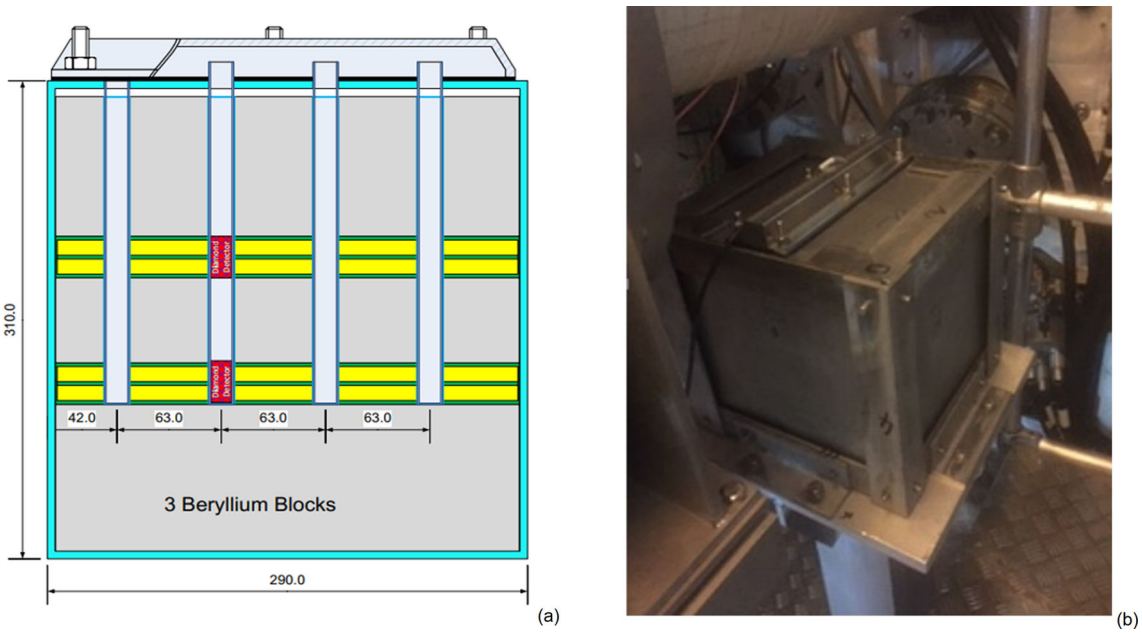

Fig. 1 Vertical cross sections of HCPB TBM mock-up (**a**) and view of the HCPB TBM mock-up on the supporting structure in the vicinity of the front collimator of the beam line in Octant 8 (**b**). Dimensions are in mm

The present manuscript aims at describing and discussing test and measurements performed at JET across the DTE2 campaign, during which about 8.5×10^{20} neutrons were produced, with extremely intensive plasma pulses occurred in the last day of the campaign (maximum neutron yield per pulse was 2.1×10^{19} neutrons produced in about 7 s, thus an average plasma neutron emission rate of 3×10^{18} s-^{1} and a peak at 4.8×10^{18} s^{-1}). The experimental setup is described at first (cfr. Section 2), both from hardware (i.e., HCPB TBM mock-up, diamond detector and measuring chain) and software (i.e., control software, data management and data sharing with the control and data acquisition system of JET, a.k.a. CODAS) standpoints. Measurements and comparison against radiation transport calculations with Monte Carlo code MCNP [9] are described in Sect. 3, while Sect. 4 is related to the analysis of the critical aspects emerged and a proposal of upgrade to overcome them. Conclusions and future work are then given in Sect. 5.

2 Experimental setup

2.1 Hardware

2.1.1 HCPB TBM mock-up

The Helium Cooled Pebble Bed Test Blanket Module mock-up (HCPB TBM mock-up) [7, 8] mimics an insert of the TBM based on the HCPB concept by replicating its main characteristics. It is a 300Dx290Lx310H mm^3 welded box of stainless steel AISI 303, 5 mm thick. The box is filled with metallic beryllium (98.8% by weight pure, with major impurities of O, Fe, C, density = 1.86 g/cm^3) and it contains two steel double cassettes (12 mm high with 1 mm thick walls) filled with Li_2CO_3 powder (density = 1.12 g/cm^3, natural lithium) to reproduce as close as possible the behavior of the Li_4SiO_4 breeder ceramics of the TBM.

The three horizontal blocks of beryllium and the two flat box capsules filled with the lithium carbonate powder are shown in the vertical cross-section in Fig. 1a, respectively in grey and yellow. There are 4 channels for instrumentation as shown in the same figure, made by thin-walled tubes with beryllium inserts at 42, 105, 168 and 231 mm from the mock-up front surface. The detector is inserted in the second most distant vertical channel from the tokamak, i.e., the second channel from the left. The top cap has a rubber gasket seal to prevent any leak of the tritium produced. The HCPB TBM mock-up is located on a dedicated holder near octant eight in the torus hall (J1T), as shown in Fig. 1b. The mock-up weighs about 75 kg and the total tritium produced due to the exposure to 14-MeV neutrons during DTE2 campaign is < 2 MBq, according to calculations based on neutron irradiation measured by JET neutron monitor KN1.

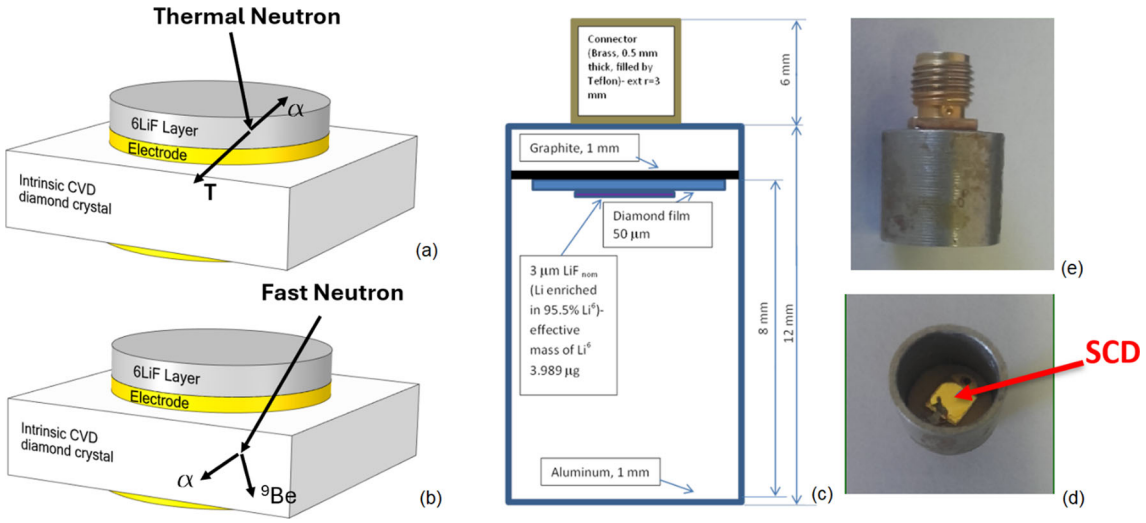

Fig. 2 Schematic view of the single crystal diamond (SCD) with electrodes and ^{6}LiF layer and the detection mechanisms for thermal (**a**) and fast (**b**) neutrons; cross-section of the TBM diamond detector with SCD, aluminum case and brass connector (**c**), view from the bottom on the gold electrode (**d**) and frontal picture (**e**)

2.1.2 TBM diamond detector

Among detectors capable of working in TBMs, Single Crystal Diamond (SCD) detectors are considered as a candidate to provide a real-time measurement of their nuclear performance through the measurement of neutron flux (and energy spectrum) and tritium production rate, both based on the detection of neutrons. This type of detector is an intrinsic artificial diamond obtained through chemical vapor deposition (CVD) [10] and the deposition of two metallic contacts on the major surfaces of the SCD for collecting electron–hole pairs created by the interaction of radiation with the crystal.

The 14-MeV neutrons produced by DT fusion reactions can be directly detected in the crystal bulk through the reaction ^{12}C(n,α)^{9}Be. The products of the reaction have a total energy $E_\alpha + E_{\mathrm{Be}} = E_{\mathrm{n}} - 5.7$ MeV, where E_{n} is the energy of the impinging neutron. The peak corresponding to such reaction is used for the detection of fast neutrons.

As for thermal neutrons, the energy threshold of the above-mentioned reaction being >6.1 MeV, it is necessary to add a ^{6}LiF coating on top of one electrode to convert neutrons into charge particles. In facts, the ^{6}LiF interacts with thermal neutrons through the nuclear reaction ^{6}Li(n,α)T thus producing 2.7 MeV tritons and 2.1 MeV alphas, which release their energy into the crystal bulk. Tritium and α peaks are used for the detection of thermal neutrons. In Fig. 2, the neutron detection mechanism is sketched for thermal (a) and fast (b) neutrons.

The SCD employed to make the detector is a 4.3×4.3 mm^2 CVD crystal, 50 µm thick [11]. Electrodes are made of gold, 100 nm thick, with a diamond-like-carbon junction [12]. The ^{6}LiF layer, on top of one of the two electrodes, is disk shaped, 3 mm diameter and 3.5 µm thick. ^{6}Li enrichment is 95% by weight. The SCD is placed inside a 1-mm-thick aluminum case and connected to the measuring chain by a connector made of brass (cfr. Figure 2).

The TBM diamond detector was calibrated to measure tritium production inside the mock-up. The calibration is described in detail in a EUROfusion report [13] and the main outcomes published elsewhere [11]. Here, and for the sake of completeness, some key elements of the calibration are recalled, including the characteristic limits of the measurement [13], as they reflect on the performance of the detector.

The calibration was performed at the thermal neutron flux density standard facility [14] of the Italian National Institute of Ionizing Radiation Metrology [15] of ENEA. Six ^{241}Am-Be neutron sources (in red in Fig. 3) with an individual neutron emission rate of about ten^{6} s^{-1} are placed in a polyethylene reflector (in green in Fig. 3). The detector is inserted into the cavity at the center of the 25 cm diameter cylinder (in blue in Fig. 3), 20 cm high, made of graphite, surrounded by a 13.5 cm thick reflector of polyethylene. An outer layer of graphite bricks acts as moderator and shield. The standard was calibrated in 1974 by means of the gold foil activation technique giving a thermal flux of 1.217×10^4 cm^{-2} s^{-1} with 0.9% of uncertainty [14], while a more recent thermal neutron flux measurement campaign occurred in 2014, reported 1.15×10^4 cm^{-2} s^{-1} ($\pm 1\%$) and this measurement was employed for the calibration of the diamond detector.

Considering that the number of ^{6}Li(n,T)α reactions per second per atom of ^{6}Li (i.e., isotopic reaction rate of the detector, R_{Li6}) is equal to the product of the cross section σ of the reaction multiplied by neutron flux φ and averaged over the neutron energy

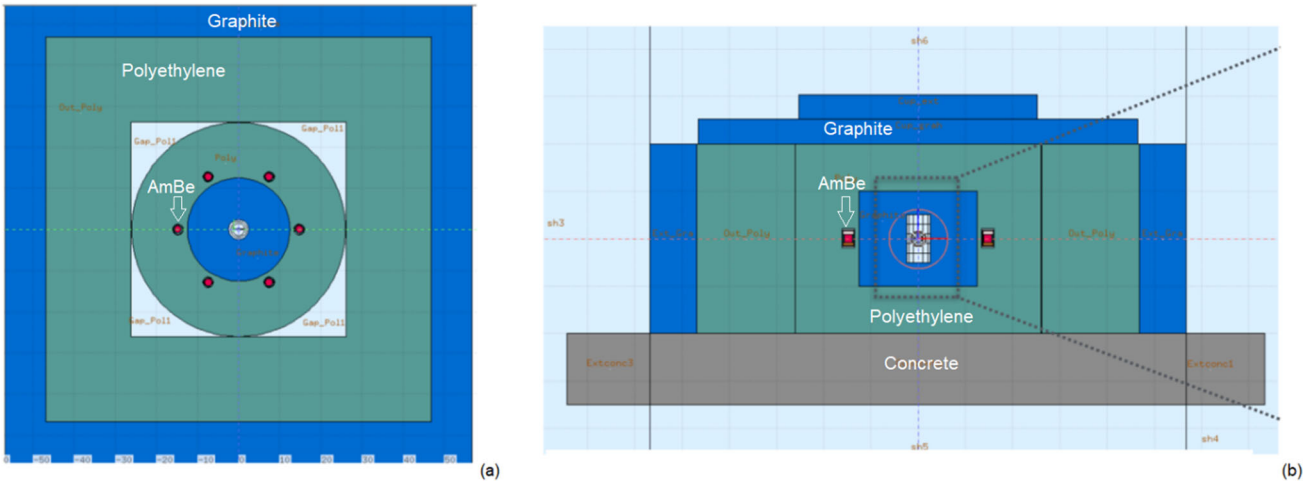

Fig. 3 ENEA-INMRI thermal neutron flux density standard: horizontal (**a**) and vertical (**b**) cross sections

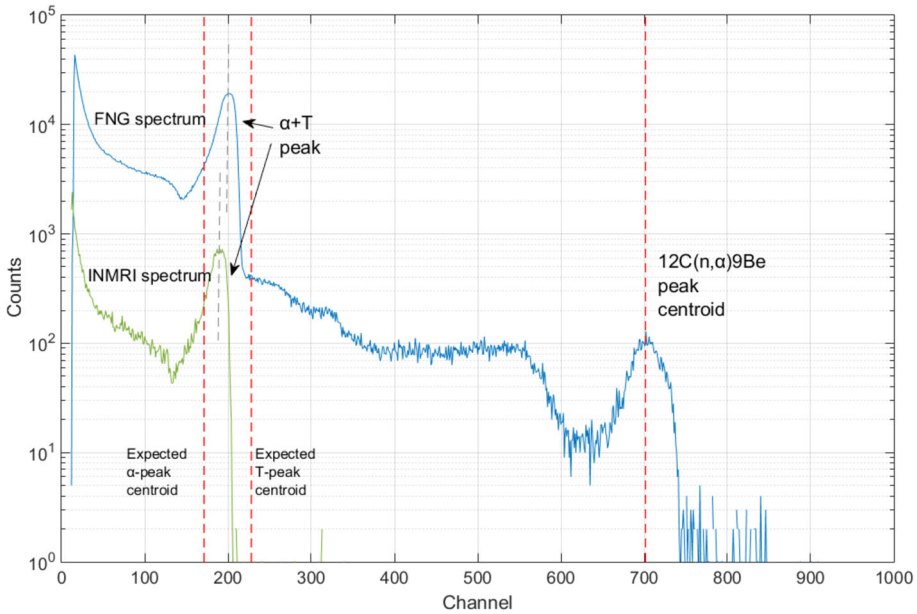

Fig. 4 Spectra acquired at the ENEA-INMRI thermal neutron facility during calibration of the diamond detector and during a test at the ENEA 14-MeV neutron generator (FNG)

spectrum, which in case of thermal neutron source can be simplified as $<\sigma\varphi> = \sigma_{th}\varphi_{th}$, the calibration factor K_{cal} is defined as follows:

$$R_{Li6} = \sigma_{th} \cdot \varphi_{th} = \frac{M_{Li6} \cdot cps}{N_{Av} \cdot m_{Li6,\,eff}} = K_{cal} \cdot cps \tag{1}$$

, where cps (counts per second) is the net count rate of the α and T peaks (due to the energy resolution of the detector, such peaks overlap), $M_{Li6} = 6.015122$ g/mol is the molar mass of ^{6}Li, N_{Av} the Avogadro number, and $m_{Li6,eff}$ is the effective mass. With respect to the real mass, the effective mass accounts also for the detection efficiency (ε) and electronics and settings of the measuring chain (k), i.e., $m_{Li6,eff} = m_{Li6}\ \varepsilon\ k$.

The spectrum acquired at the thermal neutron facility of ENEA INMRI is shown in Fig. 4 (INMRI spectrum): measurement time is 4100 s and the net count rate of the α + T peak and the characteristic limits of the measurement are in Table 1. The spectrum acquired at the ENEA 14-MeV neutron source (FNG) is shown in the same figure. During that test the detector was inserted in a polyethylene moderator so both peaks due to fast and thermal neutrons are visible. The centroid of the α + T peak in the FNG spectrum is at higher energy since neutrons are not fully thermalized as at the thermal source.

The calibration was done according to ISO 11929 [16] as reference for the measurement of the net counts, background subtraction and determination of the characteristic limits of the measurement (i.e., decision threshold, detection limit and limits of the confidence interval, cfr. Table 1). The calibration factor Kcal is determined as the ratio between $\sigma_{th}\varphi_{th}$ and cps and it amounts to $Kcal = (2.504 \pm 0.039) \times 10^{-18}$. The effective mass of ^{6}Li as determined during calibration is $m_{eff} = 3.989 \pm 0.062$ μg. Such calibration is

Table 1 Characteristic limits of the measurement

Quantity	Symbol	Value
Primary measurement result (i.e., ROI net counts)	y	17,670
Standard Uncertainty associated with y	$u(y)$	188
Decision threshold	y^*	219
Detection limit	$\boldsymbol{y}^{\#}$	440
Lower limit of the confidence level (95%)	$y^<$	17,302
Upper limit of the confidence level (95%)	$y^>$	18,038
Best estimate of the measurand	$\hat{y}$	17,670
Standard uncertainty associated with $\hat{y}$	$u(\hat{y})$	188

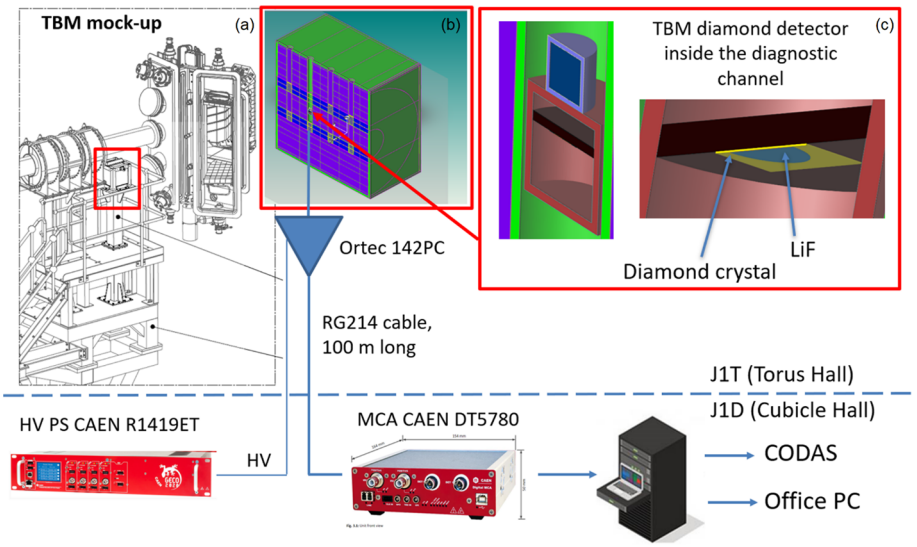

Fig. 5 Setup of TBMD diamond detection system at JET with some components installed in the torus hall (J1T) and some others in the cubicle hall (J1D). **a** 3D view of octant 8 with HCPB TBM mock-up holder framed in red; **b** cross-section of the same mock-up from the MCNP geometry model employed for radiation transport calculations; **c** magnification on the TBM diamond detector in the same geometry model

valid provided that the tritium production due to super-thermal neutrons is negligible, i.e., $<\sigma\varphi> \simeq \sigma_{\mathrm{th}}\varphi_{\mathrm{th}}$, and that the burn-up of ^{6}Li is negligible as well.

From calibration and analysis performed emerged that the proposed equipment and the procedure used to determine net counts are applicable if net counts (y) of α + T peak are larger than detection limit ($y^{\#}$), i.e., y > 440. The same considerations can be done for net count rate: the minimum count rate necessary results $y^{\#}/4100 = 0.1\ s^{-1}$. It is important to note that such values refer to the background inside the cavity of the neutron thermal source at INMRI and that the mentioned characteristic limits hold as long as radiation background at the location of the detector does not differ significantly.

2.1.3 Measuring chain

The layout of the measuring chain is shown in Fig. 5. The HCPB TBM mock-up is located on a dedicated holder near octant 8 in the JET torus hall (J1T) as shown in Fig. 5a. A vertical cross-section of the mock-up from the MCNP geometry model employed for radiation transport calculations is in Fig. 5b, including the TBM diamond detector in the second most distant vertical channel from the tokamak, shown in Fig. 5c. The detector is connected to a preamplifier ORTEC 142PC [17], located about 3 m far. The preamplifier provides high voltage (HV) to the diamond and sends the signal with improved signal/noise ratio (SNR) to the cubicle in the hall J1D through coaxial cable type RG214, about 100 m long. The preamplifier is connected to the digital multi-channel analyzer (MCA) model CAEN DT5780 [18]. HV is provided to the preamplifier by the power supply CAEN R1419ET [18]. The system is controlled from the PC located in the cubicle through a dedicated software (cfr. Sect. 2.2), both from J1D and from remote.

This layout is the result of an upgrade of the initial setup, after some tests performed on site with an alpha-emitter as radiation source and during some TT pulses before DTE2 campaign. It was originally based on the preamplifier ORTEC 142A [17], same model as the one employed during the calibration at ENEA-INMRI and replaced as faulty, and on the power supply output of the module CAEN DT5780 [18], suspected of introducing some noise in the measuring chain. Moreover, an electrical isolation transformer was installed in the cubicle to avoid any electrical disturbance from the electric grid.

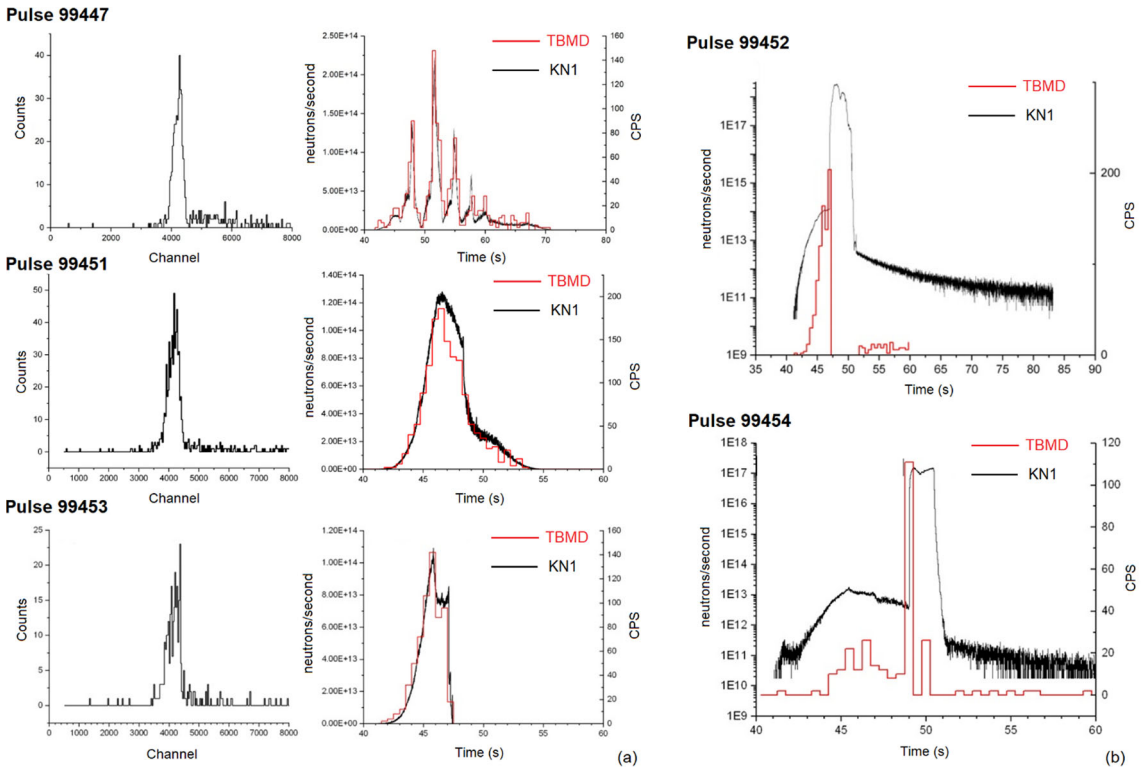

Fig. 6 **a** Energy spectrum (left column) and total cps (right column) measured by TBM diamond detector during three pulses with JET neutron emission rate $< 10^{15}$ s^{-1} (cps of diamond detector are in red and in the same plot, in black, neutron emission rate measured by KN1). **b** Total cps measured by the detector (in red) compared to the neutron rate monitor KN1 (black) during two pulses with JET neutron emission rate $> 10^{15}$ s^{-1}

2.2 Software

The software employed for managing the measurement with the TBM diamond detector is composed of three main pieces and is run in the PC in the cubicle KN5A located in J1D. It is mostly written in C++ by ENEA for the specific purpose and the main functions are as follows: (1) it starts the data acquisition after receiving the signal (JET Pretrigger) announcing a new plasma pulse from JET UDP Server; (2) it performs data acquisition and save the data into files; (3) it stops the data acquisition; (4) it manages data sharing with CODAS; (5) it performs post-analysis. The piece of software devoted to acquisition from MCA is based on proprietary libraries distributed by the manufacturer (i.e., CAENComm, CAENVMElibSetup, and CAENDigitizer). Acquisition is done in the so called 'list mode', i.e., for each detection event, time and signal amplitude are recorded. As for the communication with JET UDP Server, a second piece of software receives information on the forthcoming plasma pulse, including shot number and the pretrigger signal and gives such information to the acquisition software. Once plasma pulse is completed, the same acquisition software stores the data locally and prepare the data to be transferred to CODAS database. Starting from list mode files, a post-analysis piece of software allows to perform data elaboration to investigate the functioning of the system, including the study of the time correlation with JET neutron monitor KN1 by comparing neutron emission rate and TBM diamond detector count rate across the plasma evolution, calculation of the neutron energy spectra at different time intervals and counts of the α + T peaks from which tritium production is measured.

3 Measurements and comparison against MCNP prediction

The neutron detection performance of the system was explored across DTE2 campaign and here some significant JET pulses are considered. An important characteristic of the detection system in the present configuration is the maximum neutron emission rate of JET under which the detector can operate, about 10^{15} s^{-1}. As a matter of fact, in Fig. 6a, the energy spectrum, where the α + T peak is visible (left column) and total cps (right column) during the pulse evolution are depicted for three pulses (# 99447, 99451, 99453) with neutron rate $< 10^{15}$ s^{-1}. Total cps measured by the TBM diamond detector (in red) are compared to the neutron emission rate (in black) measured by the JET neutron monitor KN1. In Fig. 6b, total cps and neutron rate are plotted for two pulses (# 99452, 99454) when the mentioned emission rate was exceeded.

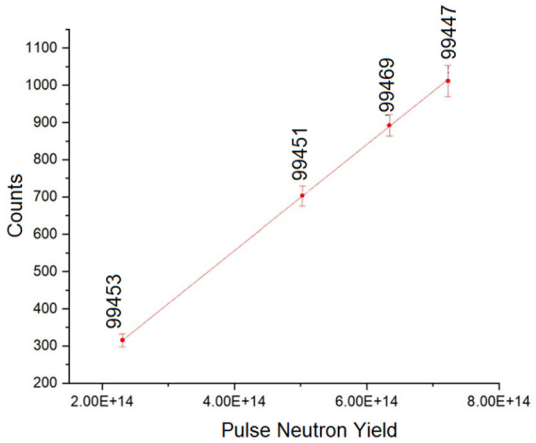

Fig. 7 Counts during pulses # 99453, 99451, 99469, 99447 measured by the TBM diamond detector as a function of the pulse neutron yield

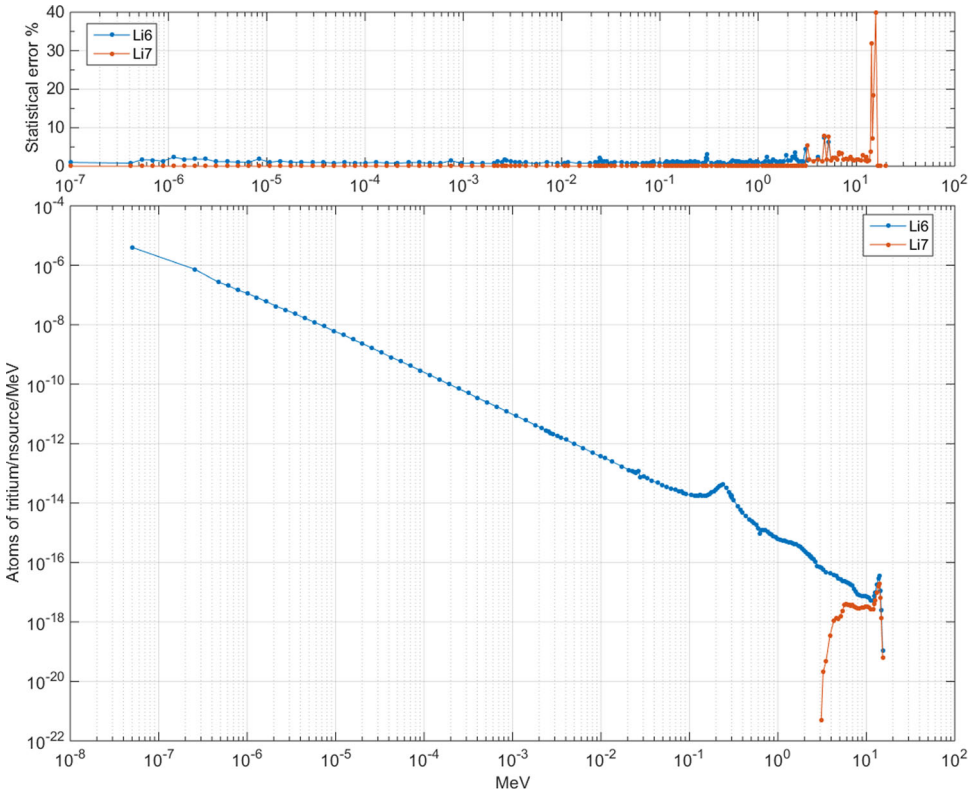

Fig. 8 Energy spectrum of the tritium production in Li6 and Li7 (bottom) and statistical errors (top)

As far as emission rate is below 10^{15} s^{-1}, the number of total cps of the TBM diamond detector are closely superimposed to the neutron monitor KN1, showing that with a certain detection efficiency, neutrons are properly detected along the pulse evolution. At higher rates, a saturation of the detector output is observed preventing the system from the proper measurement of the tritium production. Moreover, a constant detection efficiency is observed as far as neutron yield rate $< 10^{15}$ s^{-1}, as shown in Fig. 7, where the number of counts measured by the detection system are plotted as a function of the neutron yield for some JET pulses (# 99453, 99451, 99469, 99447). A clear linear trend is observed.

Three pulses are considered here for the comparison between calculations (C) and experimental results (E). Three-dimensional MCNP [9] simulations were carried out using the 360° JET model with FENDL3.1d [19] nuclear data library under DT neutron emission from JET plasma [20]. The neutron spectra have been calculated in both diamond crystal and LiF layer and the tritium production due to Li6 and Li7 in LiF layer. Weight-window bounds (i.e., a typical method to improve Monte Carlo sampling in MCNP) generated by ADVANTG code [21] have been employed to improve the accuracy and precision of the tally estimates (with respect to an analog simulation and same computation time). The energy spectra of the reaction rates of tritium production are shown in Fig. 8. The expected tritium production in LiF layer is $(1.0828 \pm 0.0049) \times 10^{-12}$ T/n_{source} due to ^{6}Li and $(4.8061 \pm 0.2259) \times 10^{-17}$ T/n_{source} due to ^{7}Li. Tritium production due to ^{7}Li is 5 orders of magnitude below the one due to ^{6}Li, so totally negligible.

Table 2 C/E calculation for three pulses measured during DTE2

Pulse number	Neutron yield	MCNP calculation		TBMD measurements	C/E for Li6	Note
		T/neutron source in Li6	T/neutron source in Li7	T/neutron source in Li6		
99447	7.23E+14	1.083E−12	4.81E−17	1.40E−12	0.77 (±0.05)	
99451	5.03E+14	1.083E−12	4.81E−17	1.40E−12	0.77 (±0.05)	
99453	2.31E+14	1.083E−12	4.81E−17	1.36E−12	0.79 (±0.06)	Below detection limit

Table 3 Uncertainty of C/E

Sources of uncertainty	99447	99451	99453
MCNP (statistical error)	0.0045	0.0045	0.0045
Calibration of TBMD	0.0156	0.0156	0.0156
Counts	0.0315	0.0377	0.0563
Calibration of KN1	0.0500	0.0500	0.0500
Uncertainty (1-sigma, %)	6.13	6.47	7.71

The calculation of C/E for pulses 99447, 99451 and 99453 is given in Table 2. The tritium production measured by the TBM diamond detector (normalized for the neutron yield of the pulse) is 1.40×10^{-12} tritons per neutron emitted for the first two pulses shown in Table 2 above the detection limit (cfr. Table 1) and 1.36×10^{-12} for the pulse below that number of counts. Sources of relative uncertainty are shown in Table 3.

As regards C, only the statistical error due to Monte Carlo sampling is accounted, while calibration of the detector, number of counts of TBM diamond detector and calibration of the neutron diagnostic KN1 (from which the total number of neutrons produced is taken) are the sources of uncertainty considered for E. Uncertainty of C/E is calculated as the root of the square sum of the mentioned sources. C/E equals to 0.77 for pulses 99447 and 99451 and 0.79 for pulse 99453 below the detection limit. Considering the necessary simplifications in this experiment, including the ones on the MCNP model and the calibration of the TBMD detector with a standard neutron thermal spectrum, $C/E = 0.77$ is considered a promising result. The underestimation of modeling ($C < E$) is to be understood.

4 Critical aspect and proposal upgrade

With respect to the operation conditions at JET, the application of this system to ITER TBMs would require considering all the aspects related to the higher temperature, robustness of the system, and higher neutron flux.

As for the first point, a thorough overview of the state of the art of diamond detectors at high temperature is given in [22] and the cases mentioned (e.g., 100 μm thick SCD operated up to 330 °C [23] and 65 μm thick SCD operated up to 425 °C [24]) support that higher working temperature is achieved with thinner diamond crystal. This is consistent with the fact that the efficiency of charge collection is inversely proportional to the thickness of the crystal and that at a certain temperature, a thinner crystal has larger charge collection efficiency. The main effects of the temperature are on two main components of the detector assembly, i.e., (1) the diamond crystal, where the high temperature could act on the transport properties of electrons and holes produced by radiation and transported toward the respective electrodes driven by the external electric field; (2) the cable which connects the detector to the preamplifier located nearby. Insulating materials employed in coaxial cables working at room temperature, as polyethylene, are not suitable to operate at high temperature, their melting point being slightly above 100 °C. An insulator as alumina, instead, employed in mineral-insulated cables, allows to hold the HV between the inner central conductor biased at hundreds V and the outer grounded conductor even at high temperature (e.g., see [22]). However, despite capable of withstanding high temperature, the insulating properties of such mineral-insulated cables degrade as temperature rise and the increase of leakage current must be accounted and understood if still compatible with the measurement. As an example, in alumina cables, the decrease of electric resistivity at 300 °C, w.r.t. room temperature, results in an enhancement of the leakage current by 4 orders of magnitude. The adoption of a mineral-insulated cable is considered necessary to operate TBM diamond detector at high temperature, provided the leakage current is small enough not to affect the measurement.

As for robustness of the system, considering the limited accessibility during ITER operation to counteract some malfunctions, stable electrical connections between components resistant to vibrations and soft accidental impact during installation and operations are to be preferred. The fragility of mineral-insulated cable must be considered also in every phase of their usage. In this respect, the current detector assembly needs a revision to improve its reliability. As an example, during a test after the initial installation, the central pin which connects the biased electrode of the detector to the inner conductor of the cable was found not firmly connected to the coaxial cable, thus breaking the electrical continuity.

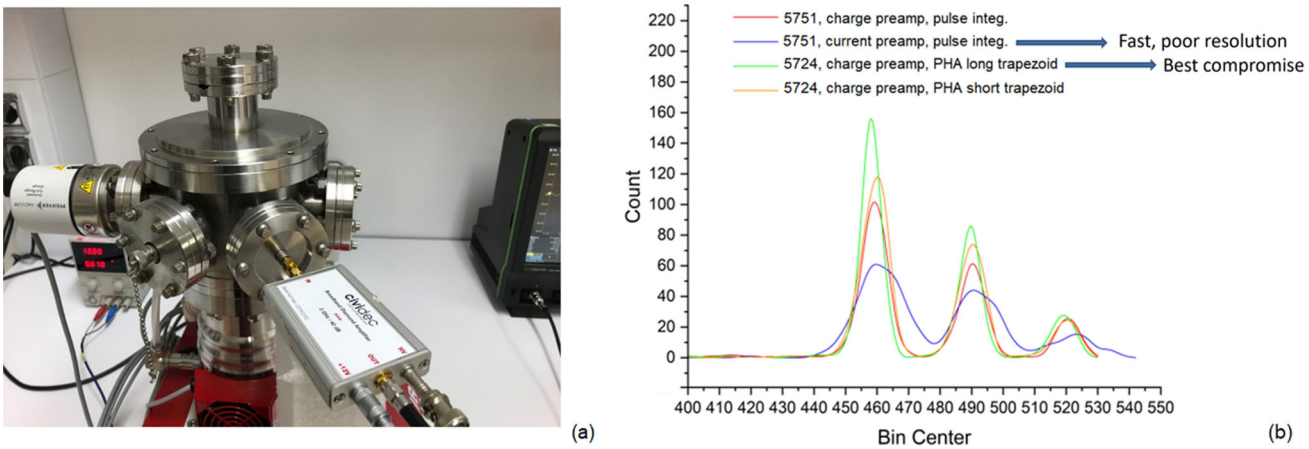

Fig. 9 **a** Setup of the vacuum chamber inside which a commercial diamond detector was exposed to alpha radiation as source of signals to test some alternative measurement chains based on a Cividec charge preamplifier and a current amplifier (four combinations of amplifier, digitizer and algorithm for the analysis were tested). **b** Energy spectra of the alpha source as recorded with the four combinations as in the legend to compare energy resolution

Table 4 Components of the four measuring chains tested, pulse width and expected maximum count rate

Amplifier type	Digitizer type	Pulse analysis type	Pulse width (ns)	Max count rate ($\times 10^3$)
Cividec Cx	CAEN Dt5751	Pulse integration	500	400
Cividec C2-HV	CAEN Dt5751	Pulse integration	30	6500
Cividec Cx	CAEN Dt5724	Pulse height (long trapezoid)	800	250
Cividec Cx	CAEN Dt5724	Pulse height (short trapezoid)	500	400

Concerning the neutron flux, in ITER TBMs it is expected about 500–1000 times the flux as in the TBM mock-up during the most intense DTE2 pulses. To adapt the system to such a high neutron flux, it is necessary to act both on the detection efficiency of the TBM diamond detector and on the maximum cps rate. The detection efficiency on thermal neutrons (here intended as cps-to-thermal-neutron-rate ratio) should be lowered and for this, the reduction of the number of ^{6}Li atoms in the LiF converting layer is the most effective measure, by reducing the thickness of the layer or by employing natural Li instead of 95% enriched. As for the maximum cps rate, apparently, the measuring chain of the TBM diamond detector is not sufficiently fast to process each detection event thus causing a pile-up of pulses as the plasma neutron emission rate exceeds 10^{15} s^{-1}. It is believed that the charge preamplifier is the bottleneck of the measuring chain in terms of processing time of the detection events. Some laboratory tests were done to assess the speed of signal processing with some alternative measurement chains (built by some combinations of digitizer, preamplifier and algorithms for pulse analysis). The most sensitive component in this comparison is the amplifier and the two models employed were the Cividec [25] current amplifier C2-HV and the charge preamplifier Cx. Tests to assess the quality of signal processing through the combinations explored were made by employing a commercial diamond detector exposed to Pu-239 Am-241 Cm-244 alpha source inside a vacuum chamber, see Fig. 9a, to limit interaction of alpha particles with air, so the spread of the energy deposited by alphas into the crystal.

In Table 4, the four configurations are compared. Pulse width is the time length of the detection pulse as shaped by the amplifier and it is extremely important to determine the maximum count rate. By assuming as maximum acceptable pile-up probability equal to 20% and a Poisson distribution of the occurrence of pulses, the maximum count rate reachable is calculated as shown in the last column.

The combinations based on charge preamplifier and long trapezoid algorithm for pulse analysis resulted the best compromise between energy resolutions (cfr. Figure 9b) and maximum count rate (cfr. Table 4). For this, it was proposed to replace the preamplifier ORTEC 142PC with a charge preamplifier Cividec as close as possible to the characteristics of the one employed during the test (i.e., model Cx [25]) to upgrade the detection system before DTE3 campaign.

5 Conclusions and future work

The tritium production measured by the diamond detector inside TBM mock-up (normalized for the neutron yield of the pulse) is 1.40×10^{-12} tritons per neutron emitted as far as the net number of counts is above the detection limit. For pulses 99447 and 99451, which produced a net number of counts above the detection limit, the ratio calculation to measurement (*C/E*) equals to 0.77. The

same ratio is higher for pulse 99453 which is below the detection limit ($C/E = 0.79$). Accounting for the necessary simplifications introduced in the nuclear model of such a complex machine as JET, uncertainty on the nuclear data on which calculations are based and the conditions under which the calibration was performed (i.e., a standard neutron thermal spectrum), $C/E = 0.77$ is considered a promising result. The underestimation of modeling with respect to the measurement ($C < E$) is to be understood.

In view of the application of the system to ITER TBMs, the critical aspects to be faced are mainly the ones related to high temperature, robustness of the system, and higher neutron flux with respect to the JET case. The adoption of a mineral-insulated cable is considered necessary to operate TBM diamond detector at high temperature and, despite the good insulating properties of high temperature insulating materials as alumina, the design of the cable must aim at reducing the leakage current through the same insulating layer at a level sufficiently low not to affect the measurement. As for robustness of the system, stable electrical connections between components resistant to vibrations and soft accidental impact during installation or operations are to be preferred for this kind of application. Concerning the neutron flux, since in ITER TBMs it is expected about 500–1000 times the flux as in the TBM mock-up during the most intense DTE2 pulses, it is necessary to act both on the detection efficiency of the detector and on the maximum cps rate. The detection efficiency can be lowered by reducing the thickness of the LiF converting layer or by employing natural Li instead of 95% enriched in ^{6}Li.

To increase the maximum count rate, since the measuring chain of the TBM diamond detector is not sufficiently fast to process each detection event thus causing a pile-up of pulses as the plasma neutron emission rate exceeds 10^{15} s^{-1}, it is necessary to act on the bottleneck of the chain in terms of processing time of the detection events, i.e., the preamplifier.

Some laboratory tests were done to assess the speed of signal processing with some alternative measurement chains, built by some combinations of digitizer, preamplifier and algorithms for pulse analysis. The most effective upgrade of the current system would be the installation of a faster preamplifier. It is proposed to replace the preamplifier currently installed (ORTEC 142PC) with a charge preamplifier Cividec Cx, to increase the maximum count rate up to 2.5×10^5 s^{-1} and to test it during the subsequent JET campaigns.

Acknowledgements This work has been carried out within the framework of the EUROfusion Consortium, funded by the European Union via the Euratom Research and Training Programme (Grant Agreement No 101052200—EUROfusion). Views and opinions expressed are however those of the author(s) only and do not necessarily reflect those of the European Union or the European Commission. Neither the European Union nor the European Commission can be held responsible for them.

Funding Open access funding provided by Ente per le Nuove Tecnologie, l'Energia e l'Ambiente within the CRUI-CARE Agreement.

Data availability statement The manuscript has associated data in a data repository. The datasets generated during and/or analyzed during the current study are available from the corresponding author on reasonable request.

References

1. M. Keilhacker et al., High fusion performance from deuterium-tritium plasmas in JET. Nucl. Fusion **39**, 209 (1999). https://doi.org/10.1088/0029-5515/39/2/306
2. J. Jacquinot et al., Overview of ITER physics deuterium-tritium experiments in JET. Nucl. Fusion **39**, 235 (1999). https://doi.org/10.1088/0029-5515/39/2/307
3. J. Paméla et al., The JET programme in support of ITER. Fusion Eng. Des. **82**, 590–602 (2007). https://doi.org/10.1016/j.fusengdes.2007.03.003
4. J. Mailloux et al., Overview of JET results for optimising ITER operation. Nucl. Fusion **62**, 042026 (2022). https://doi.org/10.1088/1741-4326/ac47b4
5. P. Batistoni et al., Technological exploitation of Deuterium-Tritium operations at JET in support of ITER design, operation and safety. Fusion Eng. Des. **109–111**, 278–285 (2016). https://doi.org/10.1016/j.fusengdes.2016.03.012
6. X. Litaudon et al., Eurofusion contributions to ITER nuclear operation. Nucl. Fusion (2024). https://doi.org/10.1088/1741-4326/ad346e
7. P. Batistoni et al., Neutronics experiment on a helium cooled pebble bed (HCPB) breeder blanket mock-up. Fusion Eng. Des. **82**, 2095–2104 (2007). https://doi.org/10.1016/j.fusengdes.2007.04.009
8. P. Batistoni et al., Neutronics experiments for uncertainty assessment of tritium breeding in HCPB and HCLL blanket mock-ups irradiated with 14 MeV neutrons. Nucl. Fusion **52**, 083014 (2012). https://doi.org/10.1088/0029-5515/52/8/083014
9. MCNP X-5 Monte Carlo Team, MCNP – A General Monte Carlo N-Particle Transport Code Overview and Theory (Version 5, vol. I), Los Alamos National Laboratory, Report LA-UR-03–1987, 24 April 2003 (Revised 3.10.05)
10. R.S. Sussman (Editor), CVD Diamond for Electronic Devices and Sensors, John Wiley & Sons, Ltd., 2009, ISBN: 978-0-470-06532-7
11. M. Angelone et al., Calibration and test of a 6LiF-diamond detector for the HCPB mock-up experiment at JET. Fusion Eng. Des. **146**, 1755–1758 (2019)
12. A. Galbiati et al., Performance of monocrystalline diamond radiation detectors fabricated using TiW, Cr/Au and a novel ohmic DLC/Pt/Au electrical contact. IEEE Trans. Nucl. Sci. **56**(4), 1863 (2009)
13. N. Fonnesu et al., Preliminary calibration of SCD detectors for Tritium measurements, EUROfusion Engineering Grant 2015 Deliverable Report D3, June 2018
14. E. Rotondi et al., Thermal neutron flux density standard at C.S.N. Casaccia: design and calibration, Energ. Nucl. (Milan), v. 21, no. 1, pp. 53–55 (1974)
15. https://www.inmri.enea.it/en/metrology, Internet site accessed in June 2024

16. ISO, 2010. ISO 11929 Standard. Determination of the Characteristics Limits (Decision Threshold, Detection Limit and Limits of the Confidence Interval) for Measurements of Ionizing Radiation – Fundamentals and Application
17. ORTEC, https://www.ortec-online.com, Internet site accessed in June 2024
18. CAEN, https://www.caen.it, Internet site accessed in June 2024
19. FENDL: A library for fusion research and applications, Nuclear Data Sheets 193 (2024), 1–78
20. R. Villari et al., Final Report on Deliverable TBMD-E24 (ENEA Contribution), Pre-analysis of TBM mock-up experiment, EUROfusion WPJET3, May 2020
21. S.W. Mosher et al., ADVANTG-An Automated Variance Reduction Parameter Generator, ORNL/TM-2013/416 Rev. 1, Oak Ridge National Laboratory, 2015
22. M. Angelone et al., Properties of diamond-based neutron detectors operated in harsh environments. J. Nucl. Eng. **2**(4), 422–470 (2021). https://doi.org/10.3390/jne2040032
23. M. Angelone et al., Systematic study of the response of single crystal diamond neutron detectors at high temperature. J. Instrum. **15**, P03031 (2020). https://doi.org/10.1088/1748-0221/15/03/P03031
24. R. Pilotti et al., Development and high temperature testing by 14 MeV neutron irradiation of single crystal diamond detectors. J. Instrum. **11**, C06008 (2016). https://doi.org/10.1088/1748-0221/11/06/C06008
25. https://cividec.at, Internet site accessed in June 2024